Optimization of an Industrial Aerobic Bioreactor Using Combined CFD, Scale-Down, and Experimental Techniques

Esmaeilnejad Ahranjani, Parvaneh*+

Department of Anaerobic Bacterial Vaccine Research and Production, Razi Vaccine and Serum Research Institute, Agricultural Research, Education and Extension Organization (AREEO), P.O. Box 31975/148, Karaj, I.R. IRAN

Noofeli, Mojtaba

Research and Development Department, Razi Vaccine and Serum Research Institute, Agricultural Research, Education and Extension Organization (AREEO), P.O. Box: 31975/148, Karaj, I.R. IRAN

Faramarzi, Ardeshir

Department of Human Bacterial Vaccine Production, Razi Vaccine and Serum Research Institute, Agricultural Research, Education and Extension Organization (AREEO), P.O. Box: 31975/148, Karaj, I.R. IRAN

ABSTRACT: *The dissolution of oxygen into the fermentation medium and the appropriate mass transfer conditions are of crucial importance in designing large-scale aerobic bioreactors. The investigation of mass transfer rates and flow structures in a large-scale process by only using experimental methods is hardly feasible, more likely because of the huge running costs. Also, those investigations by only using simulation approaches would not be accurate. Thus, this study is devoted to the application of a facile hybrid simulation/scale-down/experimental approach to optimize the structure and operation of a 400-L bioreactor used for the diphtheria bacteria culture. Assisted by the Computational Fluid Dynamics (CFD) simulation, the effects of engineering parameters such as the type, agitation rate, and location of the impeller, viscosity as well as the airflow rate and inlet place on the hydrodynamics of large-scale bioreactor were studied. Using the Concaved Blade Disc Turbine (CBDT) impeller located at the 30-cm distance with an agitation rate of 550 rpm as well as the air inlet placed at the bottom with a flow rate of 20 L/min, a superior improvement in air distribution, bubbles size, and k_La value (0.64 s^{-1}) was observed. To verify the simulation results, 15-L bench-scale bioreactors were developed by using a scaled-down (equivalent volumetric power (P/V)) strategy. The CFD simulation results implied that the bench-scale and large-scale bioreactors have comparable hydrodynamic environments. Additionally, the k_La values obtained experimentally were very close to the ones got by the simulation. These results make the CFD-assisted optimized 400-L bioreactor a potential candidate for this bioprocess.*

KEYWORDS: *CFD simulation; Bioreactor Scale-down; Optimization; Air holdup; Oxygen transfer coefficient.*

INTRODUCTION

The proper design of bioreactors in both research and industrial scales is a necessity in order to achieve optimal product formation [1-4]. This means that their operational conditions and hydrodynamic environment must be precisely controlled, which requires comprehensive knowledge of the mass transfer, and mass, momentum, and energy balances [5,6]. Such an investigation using experimental techniques is extremely time-consuming and high-costing. Hence, rapid and low-cost modeling approaches like the CFD simulation are recommended to accurately predict the complex performance of bioreactors [7-10]. Additionally, this tool can address the difficulties of placing probes in a system in order to measure the critical parameters. Since the performance of different biological systems is not similar, there are various research works focused on the optimization of a particular bioprocess.

As the mixing crucially influences the distribution of air [11-13], it has been studied the effect of the impeller types such as Combijet, Phasejet, and Rushton on the mass transfer in a 200-L vessel [14]. By performing experimental analysis, it was reported that the accuracy of the results obtained for the Rushton impeller was higher than those predicted for other impellers. *Botlagunta et al.* [15] reported that the Rushton impeller can result in higher k_La in a bioreactor, as compared to others including the paddle, marine, segmented, and elephant ear impellers. By using the CFD approach, *Bezzo et al.*[16] confirmed the feasibility of the operation control and the design of the geometry, impeller, and baffle of a reactor utilized for xanthan gum production. Also, through studying the local values of the gas holdup, oxygen bubbles diameter, and gas-liquid mass transfer coefficient of a stirred tank (5 L), it has been suggested that CFD simulation using the Luo and Svendsen's model can predict reasonable results [17]. In other reports, it has been shown that, for a gas-liquid stirred reactor (100 L), the results of the eddy cell and slip velocity models were almost similar to the experimental ones [18]. For the scale-up of the erythromycin culture process, CFD simulation technique has been demonstrated as a reliable tool for the investigation of the relationships between the hydrodynamics and physiology of microbes [19]. Moreover, CFD technique has been successfully applied for the estimation of power number, mixing time, gas holdup, and bubble size in a reactor equipped with the Rushton impeller [18,20].

In some cases mentioned previously, the experiments have been carried out for the verification of the simulation results. However, for large-scale processes, performing experimental assays must be highly costly and time-consuming. Apart from that, the accessibility to all locations in the large systems because of the sterile conditions and turbulent multiphase flow would be difficult. To address these issues, the accuracy of simulation results must be validated by using the scale-up (down) strategies. These strategies including the volumetric power (*P/V*), impeller tip speed, impeller shear rate, and specific impeller pumping rate are used to investigate the operation of bioreactors at the bench scales and then to extend the results to the large scales [21-23]. Among these various methods, the constant *P/V* value is considered as a scaling criterion not because it is a readily measurable variable, but because no over-estimated and/or under-estimated parameters are observed upon the scale-up [8,24].

The motivation of the current work was to accurately optimize all the parameters related to the mixing and aeration in an industrial-scale bioreactor by using a handful number of experiments. Thus, by taking the fermentation of diphtheria bacteria for vaccine production as a case study, all the structural and operational parameters of a 400-L stirred bioreactor were evaluated for the improvement of the air distribution and oxygen mass transfer. To the best of our knowledge, no scientific research has been reported so far on the industrial diphtheria bacteria culture bioreactor, where a hybrid CFD/scale-down/experimental method is applied for its comprehensive optimization. The novelty and contributions of the works are summarized in these steps: (I) the hydrodynamics of the industrial-scale bioreactor is thoroughly studied by using the CFD, and an optimized design of 400-L bioreactor is suggested, (II) a scale-down approach of the constant *P/V* value is applied to design the bench-scale bioreactors, which are then investigated by the simulation and experiments, and (III) the utilized method is successfully demonstrated as a time- and resource-efficient approach for attaining the optimized large-scale bioreactor model. The sequential steps involved in the optimization of the industrial bioreactor are illustrated in Scheme 1. This study makes a great contribution to the good design of an industrial aerobic bioreactor by analyzing the effects of the viscosity, impeller type,
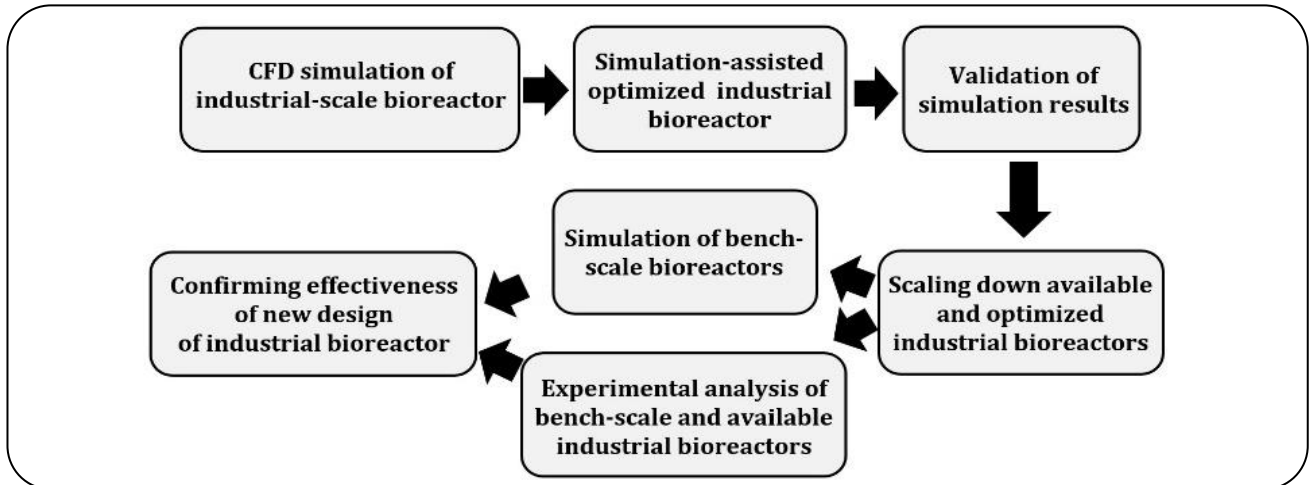
Scheme 1: Schematic illustration of the consequence of the techniques applied for the optimization of an industrial-scale bioreactor.

agitating rate, and location as well as the aeration rate and inlet place on the velocity, shear stress, air holdup, bubbles size, and k_La values.

EXPERIMENTAL SECTION

Numerical models used in CFD simulation

The operational behavior of the aerobic bioreactor utilized at Razi Vaccine and Serum Research Institute (RVSRI) was predicted using the Eulerian-Eulerian model. This bioreactor was considered as a two-phase system of air and culture media including diphtheria bacteria. In this approach, the mass and momentum balance equations were independently solved and the coupling between phases was achieved through the interphase exchange terms [25]. The mass conservation equation was expressed by using Equation (S1), in the Online Resource. Considering the existence of n phases with the volume fractions of α_i and the correlation of $\sum_{i=1}^{n} \alpha_i = 1$, the momentum conservation equation for phase i in an inertial reference frame was described by using Equation (1) [26,27].

$$\frac{\partial(\alpha_i \rho_i \vec{v}_i)}{\partial t} + \nabla \cdot (\alpha_i \rho_i \vec{v}_i \vec{v}_i) = \tag{1}$$
$$-\alpha_i \nabla p + \nabla \bar{\bar{\tau}}_i + \alpha_i \rho_i \vec{g} + \sum_{j=1}^{n} \vec{R}_{ji} + \alpha_i \rho_i (\vec{F}_i)$$

Where ρ_i is the density (kg/m³), $\vec{v}_i$ is the velocity (m/s), $\vec{F}_i$ is the external force (N), $\vec{R}_{ji}$ is the interphase force, P is the pressure (Pa), $\bar{\bar{\tau}}_i$ is the shear stress tensor (Pa), which was defined by using Equation (S2), and

$(\sum_{j=1}^{n} \vec{R}_{ji})$ is the interphase force obtained by using equations from Equation (S3) to Equation (S6).

To determine the flow regime within the stirred bioreactor, Re number was calculated by using Eq. (2) [28,29].

$$Re = \frac{\rho N D^2}{\mu} \tag{2}$$

Where ρ, N, μ, and D are the density (kg/m³), rotational speed (s⁻¹), viscosity (cp), and impeller diameter (m), respectively. In the current study, the values of Re number calculated at all agitation conditions were in the range of the turbulent flow regime. In order to model the effect of turbulence, the standard k-ε model was applied to calculate the kinetic energy and energy dissipation rate by using Equation (3) and Equation (4), respectively [30].

$$\frac{\partial(\rho_m k)}{\partial t} + \nabla \cdot (\rho_m \vec{\vartheta}_m k) = \tag{3}$$
$$\nabla \cdot \left(\frac{\mu_{t,m}}{\sigma_k} \nabla k\right) + G_{k,m} - \rho_m \varepsilon$$

$$\frac{\partial(\rho_m \varepsilon)}{\partial t} + \nabla \cdot (\rho_m \vec{\vartheta}_m \varepsilon) = \tag{4}$$
$$\nabla \cdot \left(\frac{\mu_{t,m}}{\sigma_\varepsilon} \nabla \varepsilon\right) + C_{1\varepsilon} G_{k,m} - C_{2\varepsilon} \rho_m \varepsilon$$

Where, k is the turbulent kinetic energy (m²/s²) and ε is the dissipation rate (m²/s³). The average velocity (ϑ_m), density (ρ_m), turbulent viscosity (μ_{tm}), and generation of turbulence kinetic energy ($G_{k,m}$) were defined by using the equations from Equation (S7) to Equation (S11). Also, the standard values of $\sigma_\varepsilon = 1.3$, $\sigma_k = 1.0$,

$C_\mu = 0.09$, $C_{2\varepsilon} = 1.92$, $C_{1\varepsilon} = 1.44$ were applied in Equation (3) and Equation (4).

Under the complex behaviour of the stirred fluid, the hydrodynamic forces inside the liquid phase can overcome the surface tension of the gas bubbles. This can lead to the coalescence of gas bubbles and the breakup of gas bubbles. Therefore, to determine the interphase momentum exchange and interfacial area, there is a need to predict the bubbles size distribution in the bioreactor. Considering $n(V,t)$ as the number density of bubbles of size V at time t, the PBE was expressed by using Eq. (5) [31].

$$\frac{\partial}{\partial t}[n(V,t)] + \nabla \cdot [\vec{u}n(V,t)] = \qquad (5)$$
$$B_{ag} - D_{ag} + B_{br} - D_{br}$$

The functions of B_{br}, D_{ag}, B_{br}, and D_{br} were defined by using the equations from Equation (S12) to Equation (S15).

To couple the population balance modeling of the gas phase with the overall fluid dynamics, the Sauter mean diameter (d_s, Equation (6)) was defined to evaluate bubbles diameter [7]. Also, the mass transfer coefficient of oxygen (k_La, s^{-1}) was calculated according to Higbie's penetration theory and bubble size distribution (Eq. (7)) [7].

$$d_s = \frac{\sum n_i d_i^3}{\sum n_i d_i^2} \qquad (6)$$

$$k_L a = \frac{2}{\sqrt{\pi}} \sqrt{D_{O_2}} \left(\frac{\varepsilon \rho_L}{\mu_L}\right)^{\frac{1}{4}} \times \frac{6\alpha_G}{d_s} \qquad (7)$$

Where D_{O_2} is the oxygen diffusion coefficient, ε is the turbulent energy dispassion, ρ_L is the liquid density, μ_L is the liquid viscosity, and α_G is the air holdup.

CFD simulation and conditions

The commercial CFD software (ANSYS Fluent 2019 R1) was applied to simulate the flow fields in 400-L and 15-L bench-scale bioreactors. The geometric details of the 3D bioreactors models equipped with various impellers are described in Table 1. The models and tetrahedral computational cells were generated in ANSYS Design Modeler. In order to verify the independency of results from the meshing scheme, different numerical mesh grid refinements were investigated. No-slip boundary surfaces with the standard wall functions were used for the bioreactor and impellers walls. The impellers and the agitating shaft were set as moving walls, and the other walls were kept static by default. Then, the fluid dependent k-ε turbulence model was activated. The interphase force option was set up by activating the drag force and turbulence dissipation force models. The buoyancy effect was considered by setting up the surface tension coefficient and gravitational acceleration. The governing equations for the mass, momentum, and phase balances were then solved by a finite control volume method.

The pressure-velocity coupling was obtained by using the Phase Coupled SIMPLE algorithm and Second-Order Upward schemes for the momentum and energy discretization. This was applied to obtain a good solution convergence rate. The convergence criterion, which is the sum of normalized residuals, was set to 10^{-4} for all the equations. The numerical simulations were run on a computer with Intel 12-Core CPU processor, 32 GB RAM and 64-bit operating system.

In this study, the purpose was to study the effect of (I) impeller type (*i.e.,* Rushton (RT), Concaved Blade Disc Turbine (CBDT), and paddle (PT) turbines), (II) agitation rate (R_a; 400, 550, and 700 rpm), (III) viscosity (μ; 2, 4, and 6 mPa s), (IV) impeller location (in a 20, 30, and 40-cm distance from the bottom), (V) air flow rate (F_{air}; 10, 20, and 40 L/min) and (VI) air inlet place (at the top of the bioreactor in the 30-cm radial distance, at the bottom in 30 cm radial distance, and on the wall surface in 40-cm distance from the bottom). Accordingly, five simulation steps were conducted to optimize the structural and operational parameters of the industrial-scale bioreactor (Table 2).

Scale-down procedure

The strategy of constant *P/V* value [8,24], was applied in this study to scale-down the currently-utilized industrial bioreactor and the one recommended based on the CFD simulation results. The structural and operational conditions of the currently-utilized industrial bioreactor are as follow: the RT impeller located at 20-cm distance from the bottom with the R_a of 550 rpm as well as the F_{air} of 20 L/min located on the upper surface of the bioreactor. This type of bioreactor is hereafter referred to as ISB-RT. In a brief procedure, first the *P/V* values for the as-mentioned bioreactors were calculated according to Equation (8). Then, the estimated *P/V* values were applied for the bench-scale 15-L bioreactors, which had

Table 1: The large-scale and bench-scale bioreactors as well as impellers configuration and dimensions.

Parameter	400-L Bioreactors	15-L Bioreactors
Diameter of bioreactor	76 cm	25 cm
Height of bioreactor	90 cm	31 cm
Medium volume in bioreactor	350 L	13 L
Diameter of all impellers	30 cm	9.8 cm
Thickness of all parts of turbines	5 mm	2 mm
Blade number of all turbines	6	6
Middle disk diameter of RT and CBDT	10 cm	3.2 cm
Blades angle of CBDT	45º	45º
Diameter of impeller rod	3 cm	1.1 cm
Blades length of RT and CBDT	10 cm	3.3 cm
Blades width of all turbines	10 cm	3.1 cm

the geometry and configurations similar to the large-scale bioreactors (Table 1), in order to calculate the required agitation rates. Afterward, their hydrodynamics parameters were predicted using the CFD simulation and then compared with those obtained for the large-scale bioreactors.

$$\frac{P}{V} = \frac{N_p \rho N^3 D^5}{V} \tag{8}$$

where N_p is the powe number, ρ is the media density (kg/m^3), V is the liquid volume in the bioreactor (m^3), D is the diameter of the impeller (m), N is the impeller agitation rate (s^{-1}).

Experiments procedure

To study the reliability of the scale-down method, k_La values were calculated. Briefly, the *Corynebacterium diphtheriae* cell culture process was simulated in three bioreactors, namely, the industrially utilized 400-L stainless steel bioreactor equipped with RT impeller (ISB-RT), bench-scale 15-L glass bioreactor equipped with RT impeller (BSB-RT) and bench-scale 15-L glass bioreactor with CBDT impeller (OBSB-CBDT) (see Table 1). The ISB-RT picture is presented in Fig. S1, in Online Resource. The media in the bioreactors had an initial μ of 1.4 mPa s and a density of 1500 kg/m^3 [32]. The media were depleted of oxygen by nitrogen sparging prior to introducing air flow into the bioreactors. To estimate the k_La value in these three different bioreactors, the dynamic

method was applied by using Equation (9) [15]. The dissolved oxygen concentration ([O$_2$]) was read online and then d[O$_2$]/dt was obtained by making a correlation between ([O$_2$] and time. The amount of [O$_2$] was assumed to be the same in the whole bioreactor.

$$\frac{d[O_2]}{dt} = k_La \left([O_2]^* - [O_2]\right) \tag{9}$$

The equilibrium concentration of oxygen ([O$_2$]*) was calculated by Eq. (10).

$$[O_2]^* = \frac{y_{O_2}\left(\frac{P_T}{760}\right)}{H_{O_2}} \tag{10}$$

Where P_T is the pressure at the sparger (mmHg), y_{O2} is the molar fraction of oxygen in the inlet gas flow, H_{O2} is the Henry coefficient (atm L/mol) under ambient pressure [8,24]. It was subsequently investigated whether the results obtained by using the CFD simulation were equal to the ones calculated by the experimental approach or not. Also, the k_La values estimated for the scale-downed 15-L and available 400-L bioreactors were compared to each other. In other words, it was investigated that whether the applied scale-down method could explain the hydrodynamics of an industrial-scale bioreactor or not. To investigate the effect of operational conditions on the bacterial cell damage, the above-mentioned bacterial culture process was carried out in the ISB-RT bioreactor performing under various agitation rates (400, 550, and 700 rpm). Then, the turbidity of bacterial culture suspension was measured [33,34].

Table 2: Simulation conditions applied to optimize the structural and operational parameters of bioreactor.

Simulation step	Purpose of simulation	Constant parameters
1	Effect of impeller type	R_a of 550 rpm, impeller location in 20-cm distance from bottom, F_{air} of 20 L/min, μ of 2 mPa s, and air inlet on the top
2	Effect of R_a and μ	Best impeller type selected from simulation #1, other conditions be similar to simulation #1
3	Effect of impeller location	Best impeller type and R_a selected from simulation #1 and 2, other conditions be similar to simulation #1
4	Effect of air inlet place	Best impeller type, location, and R_a selected from simulation #1, 2, and 3, other conditions be similar to simulation #1
5	Effect of air flow rate	Best impeller type, location, and R_a selected from simulation #1, 2, and 3, air inlet place selected form simulation #4, other conditions be like simulation #1
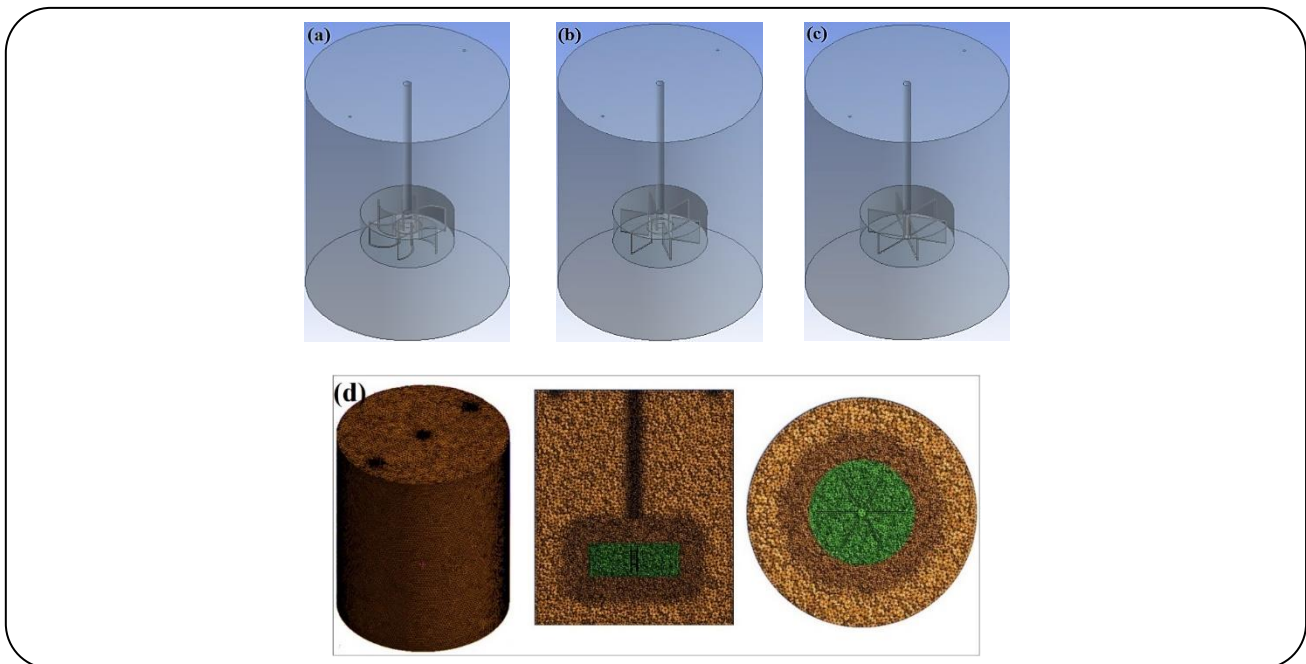
Fig. 1 Geometric models of the bioreactor with CBDT (a), RT (b), and PT (c) impellers, and computational grids of the bioreactor equipped with CBDT impeller (d).

RESULTS AND DISCUSSION

Verification of grid independency

The 3D models of industrial-scale bioreactors equipped with various impellers are presented in Fig. 1a, b, c. Three meshing schemes with different numbers of cells (1, 2.5, 5, and 7.5×10^6) were conducted for the confirmation of the independency of results from the mesh numbers. For this purpose, the bioreactor equipped with CBDT impeller located at the 20-cm distance with the R_a of 550 rpm, air inlet at the top with the F_{air} of 20 L/min, and μ of 4 mPa s was applied. The results obtained by the meshing schemes of 2.5, 5, and 7.5×10^6 cells had better independency than those obtained by the scheme of 1×10^6 cells. The v (3.43, 3.26, and 3.49 m/s, respectively) and α_G

values (4.6%, 4.7%, and 4.5%, respectively) estimated by those three schemes were quite close to each other, as compared to those obtained by the scheme of 1×10^6 cells (*i.e.*, v of 2.68 m/s and α_G of 3.1%). Since the time and cost of such computations can be limiting factors [8,35], the meshing scheme of 2.5×10^6 cells was employed in the whole study. For example, the meshed scheme of industrial bioreactor equipped with CBDT impeller is shown in Fig. 1d.

Effect of mixing-related engineering parameters

One of the important parameters significantly influences the operation of a bioreactor is the impeller type [12,13]. Therefore, the hydrodynamic environments
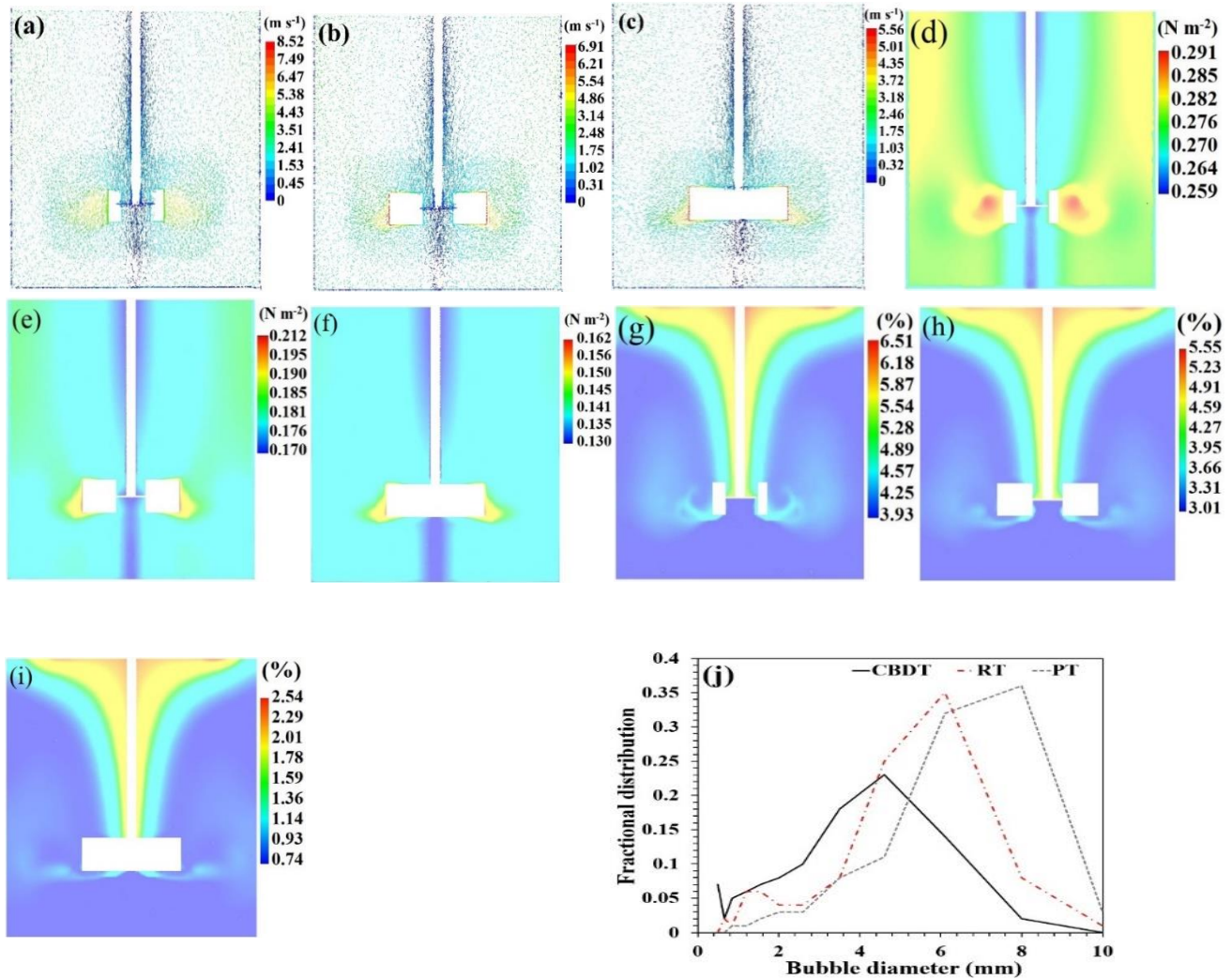
Fig. 2: The velocity vectors in bioreactors with CBDT (a), RT (b), and PT (c), τ profiles using CBDT (d), RT (e), and PT (f), αG profiles using CBDT (g), RT (h), and PT (i), and Fb in bioreactors equipped with different impellers (j).

inside the bioreactors (*i.e.*, simulation step #1, Table 2) were simulated and the results are presented in Fig. 2. The mean values of hydrodynamic parameters are listed in Table 3 as well. As seen, using the CBDT and RT impellers, the fluid flow is towards the tips of the blades, which is subsequently scattered in the whole bioreactor due to the shear stress caused by the impeller motion (Fig. 2a, b). Also, it is observed that the PT impeller creates radial fluid flow, which leads to the formation of two relatively divided domains at the top and bottom of the bioreactor (Fig. 2c). This type of flow pattern is not recommended for the mixing of two phases [8,36]. Owing to producing better velocity patterns, the CBDT and RT impellers are recommended for the suitable distribution of the gas in the liquid.

According to the shear stress profiles in these three systems (Fig. 2d, e, f), the τ value is high near the impeller blades and wall. Additionally, the τ value induced by using three impellers increases in the order of CBDT > RT > PT (Table 3). To determine the air distribution in these systems, α_G contours are presented in Fig. 2g, h, i. Using all the impellers, the lowest α_G values are seen on the areas near to the floor and wall, with the highest ones around the impellers. The average α_G value in the bioreactors increases in the order of CBDT > RT > PT (Table 3). According to the literature [28,37], the high τ values lead to the breaking of large bubbles into the small ones resulting in the long holding of air in media. These findings suggest that the appropriate v profiles and high τ values are useful for the air distribution and holding. Analyzing the

Table 3: Comparison of hydrodynamic and mass transfer parameters under different simulation conditions.

Simulation step	τ (N/m^2)	α_G (%)	d_s (mm)	$k_L a$ (s^{-1})
#1: Impeller type[a]				
CBDT	0.27	4.6	5.03	0.23
RT[b]	0.19	3.7	6.11	0.15
PT	0.14	1.1	7.23	0.04
#3: Impeller location (cm)[c]				
30	0.23	5.2	4.31	0.30
40	0.18	3.8	6.29	0.15
#4: Air inlet place[d]				
Side, in 40-cm vertical distance	0.22	6.6	3.83	0.43
Bottom, in 30-cm radial distance	0.23	7.9	3.10	0.64
#5: F_{air} (L/min)[e]				
10	0.22	4.7	2.90	0.40
30	0.23	9.2	3.48	0.66

[a] *The results reported in this step is for the impeller location of 20 cm.*

[b] *The currently utilized industrial bioreactor equipped with RT impeller.*

[c] *Air inlet place is on the top and the results for the location of 20 cm is the same reported in the first row of simulation step #1, in this table.*

[d] *F_{air} is 20 L/min and impeller is located in 30-cm distance from the bottom, so the results for the air inlet place on the top is the same reported in the first row of simulation step #3, in this table.*

[e] *Air inlet place is at the bottom, so the results for the F_{air} of 20 L/min is the same reported in the second row of simulation step #4, in this table.*

bubbles sizes can explain this theory. Fig. S2 shows that larger bubbles are presented on the wall, but the smaller ones are distributed around the impellers. In addition, the fractional distribution of bubbles (F_b) were calculated and shown in Fig. 2j. From this figure and the d_s values (Table 3), it is inferred that the bubbles size increases in the order of CBDT < RT < PT. However, the high τ, α_G, and small d_s values cannot solely represent the good operation of a bioreactor, because they are potential to lead to the foaming and decreasing of the air and media interactions [8,38]. Therefore, the $k_L a$ values were calculated to illustrate the effect of impeller type on the operation of a bioreactor (Table 3). The results indicate that the $k_L a$ values using various impellers increase in the order of CBDT > RT > PT. Owing to the high α_G, smaller d_s, and high $k_L a$ value, the CBDT impeller is applied in the next steps.

In the next step, the effects of R_a along with μ were studied (simulation step #2). During the fermentation, the enhancement of bacteria number leads to the increase of the μ of media. Therefore, considering three intervals of the fermentation process (times of 5, 15, and 30 h), which lead to the viscosities of about 2, 4, and 6 mPa s, respectively, the system was simulated and the results are

compared in Fig. 3. As seen in Fig. S3a, b, by increasing the agitation rate, the v value is enhanced. Also, Fig. 3a and Fig. S3c, d show that the increase in R_a results in the increment of τ value, which is consistent with earlier reports [8,35]. According to α_G profiles (Fig. S3e, f), the lowest α_G value is seen on the areas near the wall and the highest one exists around the impellers. By the increment of agitation rate, the α_G increases (Fig. 3b), which can be associated with the high v and τ values [8,35]. Considering both τ and d_s values (Fig. 3a, c), it is indicated that extremely high τ is not suitable for bubbles size. However, under high μ values, bubbles are broken into small ones and distributed in media for a long time. Besides, the results of the $k_L a$ values clearly indicate that the increment of the R_a from 400 to 550 rpm can be useful for the fermentation operation, though the further increment of R_a may not enhance the $k_L a$ value (Fig. 3d). As explained in the literature [8,37], it is associated with the further breaking of the bubbles and the formation of foaming. These results imply that the hydrodynamic environment in a stirred tank is quite complicated and highlights the importance of CFD simulation. As a result, because of the high α_G, small d_s, and high $k_L a$ values, the R_a of 550 rpm is selected for the next simulation steps.
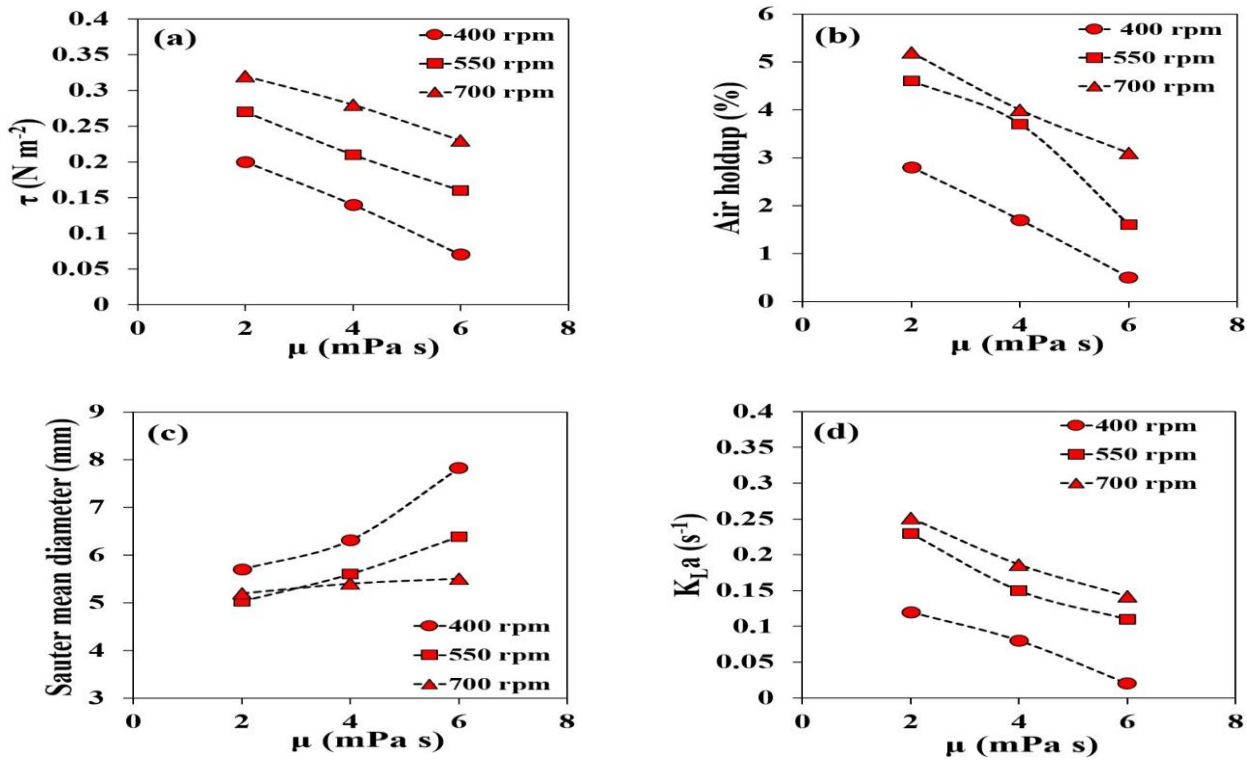
Fig. 3: The τ (a), αG (b), ds (c), and kLa (d) under various agitation rate and viscosities.

Furthermore, the bacterial culture was carried out in the ISB-RT bioreactor and the turbidity of suspension under various agitation rates (400, 550, and 700 rpm) were evaluated (Fig. S4). Under all the agitation rates, the turbidity is increased as long as the fermentation time continues up to 35 h. Comparing the results obtained at various agitation rates, it is observed that the bacterial growth increase in the order of 700 rpm ≥ 550 rpm > 400 rpm. This finding provides direct evidence that these bacterial cells are not shear sensitive, thus performing bacterial culture under agitation rates below 700 rpm can hardly damage the bacterial cells.

Fig. 4 shows the results of the third simulation step (the effect of impeller location) and the concluded parameters are listed in Table 3. Interestingly, by the alteration of impeller location, neither the v profiles were changed (Fig. S5a, b), nor the v values. From the shear stress profiles (*i.e.,* Fig. S5c in comparison to Fig. 2d) and the $τ$ values (Table 3), it is observed that locating the impeller far from the bottom results in the relatively lower $τ$ values. This reduction is particularly observed in the lower part of the impeller. As previously reported [8,12], it may be due

to the reduced relative motions. The $α_G$ profiles (Fig. 4a, b) show that the highest values are seen around the impellers as well as the areas near to the floor and wall. Also, the better air distribution and higher $α_G$ values are occurred by putting the impeller at a 30-cm distance.

Furthermore, the results of F_b (Fig. 4c) and d_s (Table 3) provide direct evidence that changing the impeller location results in an almost uniform bubbles size. The formation of larger bubbles with the impeller location of 40 cm can be attributed to the insufficient distribution of air at the lower part of the impeller, which can consequently lead to the coalescence of the bubbles around the impeller. Compared to the impeller locations of 20 and 40-cm distances, the 30-cm location offers an enhanced k_La value, fairly confirming the suitable air distribution. Owing to these results, the impeller location of 30-cm distance from the bottom is selected for the next simulation steps.

Effect of air flow-related parameters

The effects of air inlet place and F_{air} on the hydrodynamics of bioreactor are summarized in Table 3 and Fig. 5. Regardless of the air inlet place and F_{air} value,
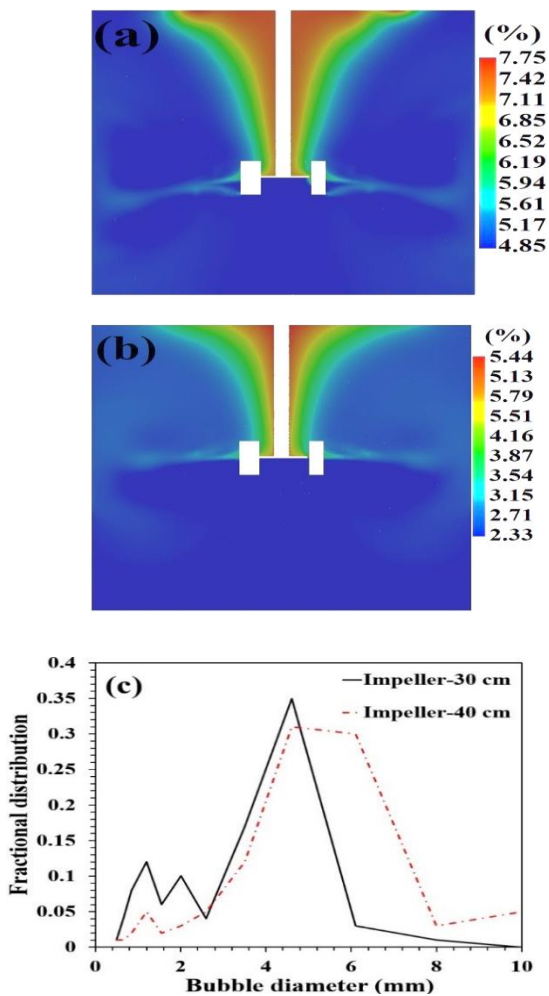
Fig. 4: The α_G profiles with the impeller location in 30 cm (a) and 40 cm (b), and F_b at different locations of impeller (c).

the v and/or τ profiles are almost similar, as illustrated in Fig. S6. This fairly indicates that these parameters are just influenced by the impeller-related parameters, as described in the previous sections. As compared to the state that the air inlet place is on the upper surface of the bioreactor, when the air inlet is located on the side, higher α_G values are achieved (Fig. 5a, b). By putting the air inlet place at the bottom, the dispersion of air is extremely increased (see Fig. 5a, b). In addition, the smaller bubble sizes are generated in the whole bioreactor when the air inlet is at the bottom (see Fig. 5e and Table 3). It implies that the possible conjugation of bubbles and the formation of foam are becoming lower under such conditions. According to Table 3, the results of k_La can also confirm the positive effect of changing air inlet place, which

provides direct evidence of the importance of the aeration from the bottom of the bioreactor.

The complicated environment of a bioreactor is also seen from the results of changing F_{air} (Fig. 5c, d, f and Table 3). According to Fig. 5c, d, the α_G value within the bioreactors is varied by the F_{air}, yet they have comparable α_G contours. Additionally, the low F_{air} (10 L/min) leads to the low α_G values and the high F_{air} (30 L/min) results in higher α_G values. However, the results of F_b (Fig. 5f) and d_s (Table 3) show that the increment of α_G in the medium possibly leads to the coalescence of air bubbles. Therefore, the k_La value obtained by F_{air} of 30 L/min, is not significantly higher than that resulting from F_{air} of 20 L/min. Owing to the results of the previous and current sections, the optimized conditions of a 400-L bioreactor are summarized to be a CBDT impeller located at the 30-cm distance with the R_a of 550 rpm. In addition, the air inlet place is suggested to be at the bottom with the F_{air} of 20 L/min. This optimized industrial-scale bioreactor using CFD simulation is hereafter referred to as 'OISB-CBDT'.

Verification of CFD simulation results

The scale-down analysis of the ISB-RT and OISB-CBDT were conducted by the means of the constant P/V value strategy (Equation (8)). In this method, the bench-scale 15-L bioreactors with configurations similar to the industrial ones (Table 1) were modelled to evaluate their hydrodynamics. The 15-L bioreactor with the configuration similar to ISB-RT is named as BSB-RT and the one with the configuration similar to OISB-CBDT is shown as OBSB-CBDT. The CFD simulation results of bench-scale bioreactors are summarized in Fig. 6 and Table 4.

Considering the figures scale bars, almost more uniform τ, α_G and F_b profiles are observed in the bench-scale bioreactors (Fig. 6), as compared to those for the industrial-scale ones (Fig. 2 and Fig. 5). However, comparing the results of BSB-RT (Table 4) with ISB-RT (Table 3) and similarly those for OBSB-CBDT (Table 4) with OISB-CBDT (Table 3), it is observed that the corresponding parameters are within acceptable and similar ranges. In addition, there is no significant difference between the results of the k_La values estimated by experiments (Equation (9)) and simulation (Fig. 6f). All these results indicate that the constant P/V value is potentially a reliable scale-down method in the presented
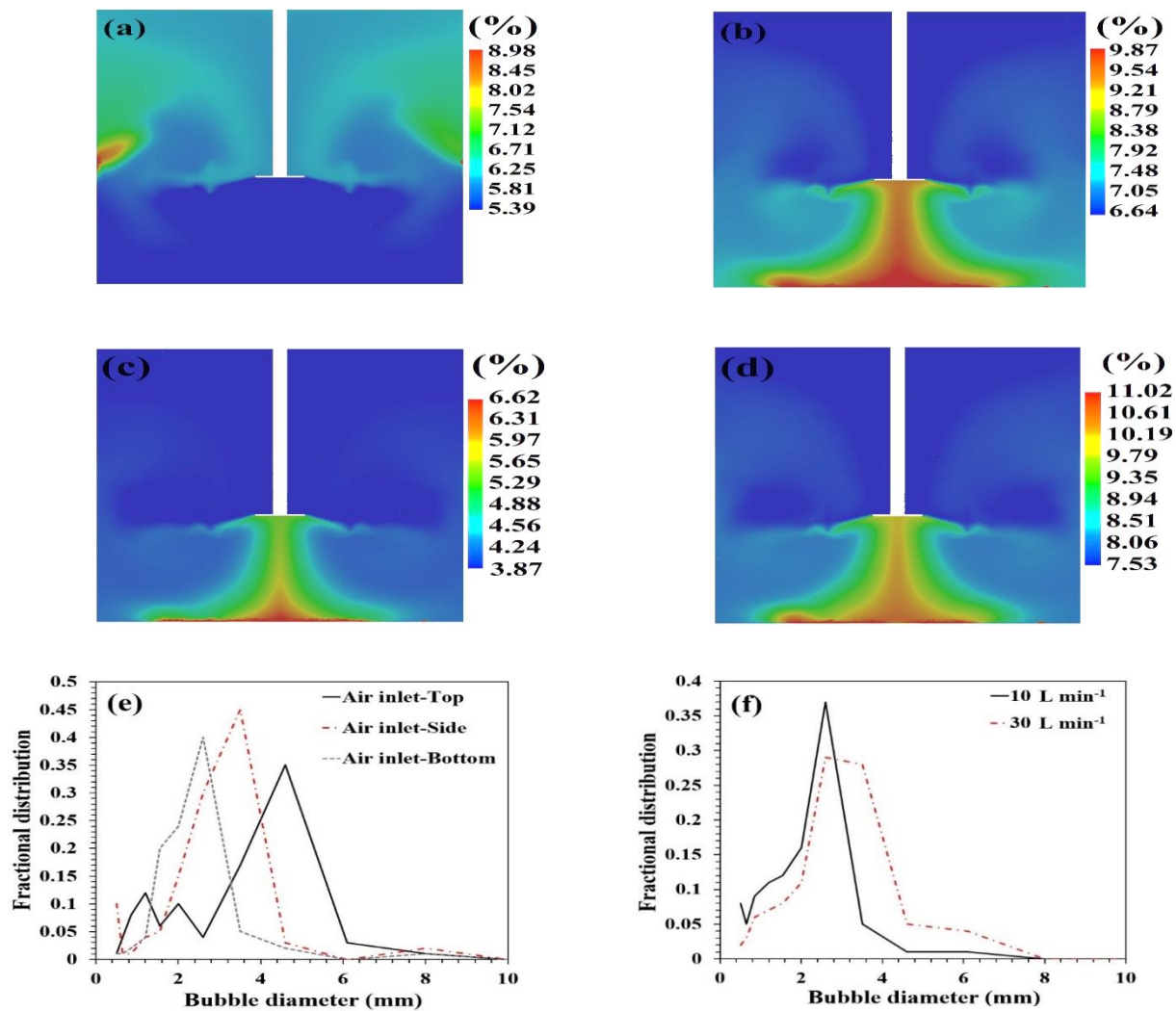
Fig. 5: The $α_G$ profiles with air inlet place on side (a) and at the bottom (b), and air flow rates of 10 L/min (c) and 30 L/min (d), as well as F_b under various air inlet locations (e) and air flow rates (f).

system, as it has been also reported in earlier reports [8,24]. In other words, these results verified that the applied scale-down method could explain the hydrodynamic environment of an industrial-scale bioreactor. Hence, the 400-L OISB-CBDT bioreactor (*i.e.,* a bioreactor with a CBDT impeller located at the 30-cm distance, and R_a of 550 rpm as well as the air inlet located at the bottom with the F_{air} of 20 L/min) can represent a good performance in case it is constructed and utilized industrially.

CONCLUSIONS

By applying the CFD simulation and experimental methods, the effects of $μ$, impeller type, location and R_a

as well as the F_{air} and air inlet place on the aerobic fermentation process in an industrial-scale bioreactor were investigated to obtain the optimal combinations of the structural and operational factors. It is observed that the CBDT impeller leads to the better v, $τ$, $α_G$, and d_s values and consequently higher k_La value, as compared to other impellers. The enhancement of the mixing rate benefits the better air distribution, the k_La value does not significantly change, however. It is also reported that the optimal location of the impeller coupled with the best air inlet place and F_{air} dramatically improves the k_La. By using a scale down strategy, the hydrodynamics of the industrial-scale ISB-RT and OISB-CBDT bioreactors are compared with

Table 4: Hydrodynamic parameters of bench-scale 15-L bioreactors obtained by CFD simulation.

Bioreactor	τ (N/m^2)	α_G (%)	d_s (mm)
BSB-RT[a]	0.15	4.1	5.67
OBSB-CBDT[b]	0.20	8.5	2.85

[a] *The bench-scale bioreactor with the configuration similar to the industrial 400-L bioreactor equipped with RT impeller (ISB-RT).*

[b] *The bench-scale bioreactor with the configuration similar to the industrial bioreactor model optimized by the CFD simulation (OISB-CBDT).*
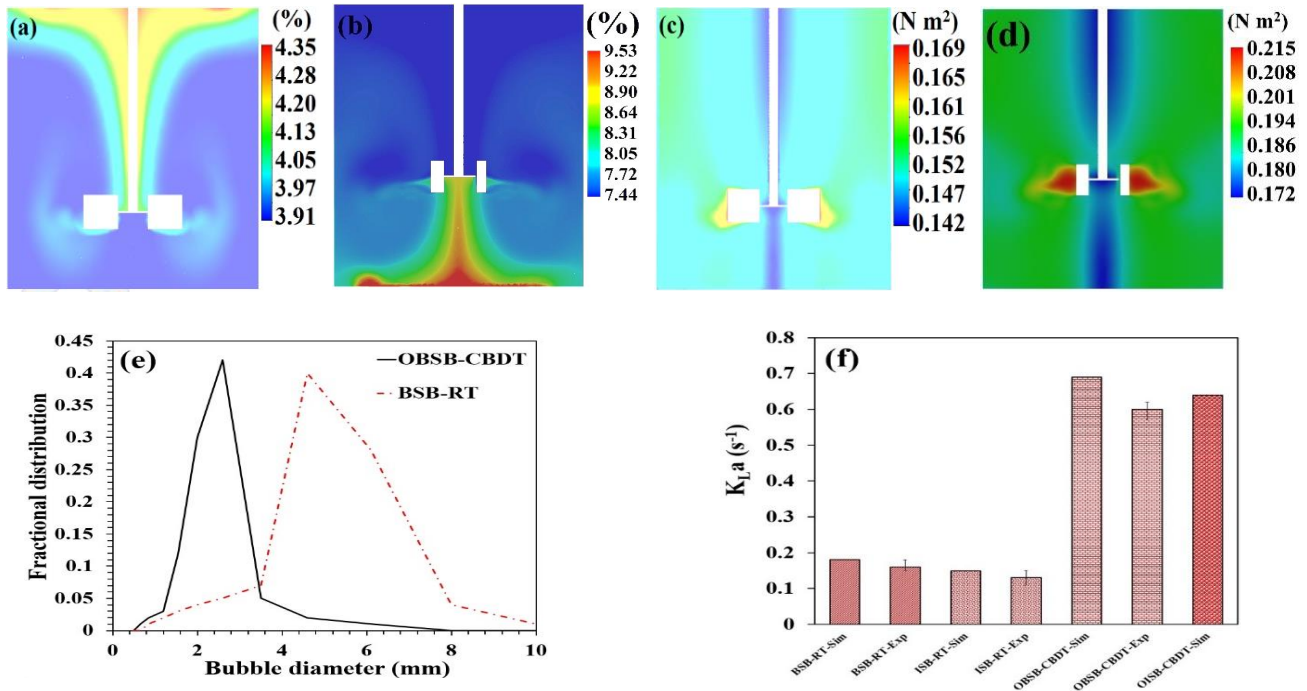
Fig. 6: The α_G profiles for BSB-RT (a) and OBSB-CBDT (b), τ profiles for BSB-RT (c) and OBSB-CBDT (d), F_b inside the bench-scale bioreactors (e), and comparison of k_La values (f) inside the currently utilized industrial bioreactor (ISB-RT), optimized one using CFD simulation (OISB-CBDT), 15-L bioreactor with configuration similar to ISB-RT bioreactor (BSB-RT), and the 15-L one with configuration similar to OISB-CBDT (OBSB-CBDT) obtained by CFD simulation (Sim) and experimental assay (Exp).

those of the bench-scale bioreactors. Almost similar performances are observed for all the bench-scale and large-scale bioreactors. Also, the k_La values obtained by the experimental analysis were very close to the ones estimated by the simulation. These results demonstrate that by using the combined scale-down simulation and experimental approaches, it can be expected that the optimized large-scale bioreactor (OISB-CBDT) result in a good operation with an effective oxygen transfer. Although the current work was focused on the optimization of diphtheria bacteria culture in an industrial bioreactor, the concluded results can be extended to other industrial bioprocesses operating in similar physical and operational conditions.

Acknowledgment

Nomenclature

RT	Rushton turbine
CBDT	Concaved blade disc turbine
PT	Paddle turbine
ISB-RT	Currently utilized 400-L industrial bioreactor
OISB-CBDT	CFD-assisted optimized 400-L bioreactor

Research Article

BSB-RT	15-L bench-scale bioreactor with configuration similar to ISB-RT bioreactor
OBSB-CBDT	15-L bench-scale bioreactor with configuration similar to OISB-CBDT
k_La	Mass transfer coefficient of oxygen, s^{-1}
d_s	Sauter mean diameter, mm
α_G	Air holdup, %
τ	Shear stress, N/m^2
v	Velocity, m/s
F_b	Fractional bubbles distribution
R_a	Agitation rate of impeller, rpm
μ	Viscosity of media, mPa s
F_{air}	Air flow rate, L/h

REFERENCES

[1] Tikhomirova T.S., But S.Y., Laboratory Scale Bioreactor Designs in the Processes of Methane Bioconversion: Mini-Review, *Biotechnol. Adv.*, **47**:107709 (2021).

[2] Pino M.S., Rodríguez-Jasso R.M., Michelin M., Flores-Gallegos A.C., Morales-Rodriguez R., Teixeira J.A., Ruiz H.A., Bioreactor Design for Enzymatic Hydrolysis of Biomass Under the Biorefinery Concept, *Chem. Eng. J.*, **347**:119-136 (2018).

[3] Esmaeilnejad Ahranjani P., Kazemeini M., Singh G., Arpanaei A., Effects of Physicochemical Characteristics of Magnetically Recoverable Biocatalysts upon Fatty Acid Methyl Esters Synthesis from Oils, *Renew. Energy*, **116**:613-622 (2018).

[4] Elmenshawe A., Abdelrazak A., Mowafey A.M., Osman Y., Optimization of Bioreactor Cultivation Parameters by Taguchi Orthogonal Array Design for Enhanced Prodigiosin Production, *Iran. J. Chem. Chem. Eng. (IJCCE)*, **39**:319-330 (2020).

[5] Nadal-Rey G., McClure D.D., Kavanagh J.M., Cornelissen S., Fletcher D.F., Gernaey K.V., Understanding Gradients in Industrial Bioreactors, *Biotechnol. Adv.,* **46**:107660 (2021).

[6] Xia J., Wang G., Fan M., Chen M., Wang Z., Zhuang Y., Understanding the Scale-up of Fermentation Processes from the Viewpoint of the Flow Field in Bioreactors and the Physiological Response of Strains, *Chin. J. Chem. Eng.,* **30**:178-184 (2021).

[7] Azargoshasb H., Mousavi S.M., Amani T, Jafari A., Nosrati M., Three-phase CFD Simulation Coupled with Population Balance Equations of Anaerobic Syntrophic Acidogenesis and Methanogenesis Reactions in a Continuous Stirred Bioreactor, *J. Ind. Eng. Chem.,* **27**:207-217 (2015).

[8] Li X.R., Yang Y.K., Wang R.B., An F.L., Zhang Y.D., Nie J.Q., Ahamada H., Liu X.X., Liu C.L., Deng Y., Bai Z.H., A Scale-Down Model of 4000-L Cell Culture Process for Inactivated Foot-and-Mouth Disease Vaccine Production, *Vaccine*, **37**:6380-6389 (2019).

[9] Zhang H., Tang S., Yue H., Wu K., Zhu Y., Liu C., Liang B., Li C., Comparison of Computational Fluid Dynamic Simulation of a Stirred Tank with Polyhedral and Tetrahedral Meshes, *Iran. J. Chem. Chem. Eng. (IJCCE),* **39**:311-319 (2020).

[10] Esmaeilnejad-Ahranjani P., Hajimoradi M., Optimization of Industrial-Scale Centrifugal Separation of Biological Products: Comparing the Performance of Tubular and Disc Stack Centrifuges, *Biochem. Eng. J.*, **178**:108281 (2022).

[11] Kazemzadeh A., Elias C., Tamer M., Lohi A., Ein-Mozaffari F., Mass Transfer in a Single-Use Angled-Shaft Aerated Stirred Bioreactor Applicable for Animal Cell Culture, *Chem. Eng. Sci.*, **219**:115606 (2020).

[12] Borys B.S., Le A., Roberts E.L., Dang T., Rohani L., Hsu C.Y.M., Wyma A.A., Rancourt D.E., Gates I.D., Kallos M.S., Using Computational Fluid Dynamics (CFD) Modelling to Understand Murine Embryonic Stem Cell Aggregate Size and Pluripotency Distributions in Stirred Suspension Bioreactors, *J. Biotechnol.,* **304**:16-27 (2019).

[13] Zheng Z., Sun D., Li J., Zhan X., Gao M., Improving Oxygen Transfer Efficiency by Developing a Novel Energy-Saving Impeller, *Chem. Eng. Res. Des.,* **130**:199-207 (2018).

[14] Moilanen P., Laakkonen M., Visuri O., Alopaeus V., Aittamaa J., Modelling Mass Transfer in an Aerated 0.2 m^3 Vessel Agitated by Rushton, Phasejet and Combijet Impellers, *Chem. Eng. J.*, **142**:95-108 (2008).

[15] Botlagunta M., Rewaria V., Mathi P., Oxygen Mass Transfer Coefficient and Power Consumption in a Conventional Stirred-Tank Bioreactor Using Different Impeller in a Non-Newtonian Fluid: An Experimental Approach, *Iran. J. Chem. Chem. Eng. (IJCCE)*, **41(2)**: 533-543 (2020).

[16] Bezzo F., Macchietto S., Pantelides C.C., General Hybrid Multizonal/CFD Approach for Bioreactor Modelling, *AIChE J.,* **49**:2133-2148 (2003).

[17] Kerdouss F., Bannari A., Proulx P., Bannari R., Skrga M., Labrecque Y., Two-Phase Mass Transfer Coefficient Prediction in Stirred Vessel with a CFD Model, *Comput. Chem. Eng.,* **32**:1943-1955 (2008).

[18] Khopkar A.R., Tanguy P.A., CFD Simulation of Gas-Liquid Flows in Stirred Vessel Equipped with Dual Rushton Turbines: Influence of Parallel, Merging and Diverging Flow Configurations, *Chem. Eng. Sci.,* **63**:3810-3820 (2008).

[19] Zou X., Xia J., Chu J., Zhuang Y., Zhang S., Real-Time Fluid Dynamics Investigation and Physiological Response for Erythromycin Fermentation Scale-Up from 50 L to 132 m^3 Fermenter, *Bioprocess Biosyst. Eng.,* **35**: 789-800 (2012).

[20] Ahmed S.U., Ranganathan P., Pandey A., Sivaraman S., Computational Fluid Dynamics Modeling of Gas Dispersion in Multi Impeller Bioreactor, *J. Biosci. Bioeng.,* **109**:588-597 (2010).

[21] Garcia-Ochoa F., Gomez E., Bioreactor Scale-up and Oxygen Transfer Rate in Microbial Processes: An Overview, *Biotechnol. Adv.,* **27**:153-76 (2009).

[22] Farrell P., Sun J., Champagne P.P., Lau H., Gao M., Sun H., Zeiser A., D'Amore T., The Use of Dissolved Oxygen-Controlled, Fed-Batch Aerobic Cultivation for Recombinant Protein Subunit Vaccine Manufacturing, *Vaccine*, **33**:6752-6756 (2015).

[23] McCoy R., Ward S., Hoare M., Sub-Population Analysis of Human Cancer Vaccine Cells-Ultra Scale-Down Characterization of Response to Shear, *Biotechnol. Bioeng.*, **106**:584-597 (2010).

[24] Xing Z., Kenty B.M., Li Z.J., Lee S.S., Scale-Up Analysis for a CHO Cell Culture Process in Large-Scale Bioreactors, *Biotechnol. Bioeng.,* **103**:733-746 (2009).

[25] Villiger T.K., Neunstoecklin B., Karst D.J., Lucas E., Stettler M., Broly H., Morbidelli M., Soos M., Experimental and CFD Physical Characterization of Animal Cell Bioreactors: From Micro- to Production Scale, *Biochem. Eng. J.*, **131**:84-94 (2018).

[26] Mavaddat P., Mousavi S.M., Amini E., Azargoshasb H., Shojaosadati S.A., Modeling and CFD-PBE Simulation of an Airlift Bioreactor for PHB Production, *J. Chem. Eng.*, **9**:562-573 (2014).

[27] Schiller L., Naumann Z., A Drag Coefficient Correlation, *VDI Zeitschrift*, **77**:318-320 (1935).

[28] Nienow A.W., Gas Dispersion Performance in Fermenter Operation, *Chem. Eng. Prog.,* **85**:61-71 (1990).

[29] Shokri A., A Kinetic Study and Application of Electro Fenton Process for the Remediation of the Aqueous Environment Containing Toluene in a Batch Reactor, *Russ. J. Appl. Chem.*, **90**: 452-457 (2017).

[30] Yufeng W., Xiaomei B., Fengxia L., Chong Z., Zhaoxin L., Study on Flow Fields in a Bioreactor with Perforated Blades, *Can. J. Chem. Eng.,* **91**:413-420 (2013).

[31] Luo H., Svendsen H.F., Theoretical Model for Drop and Bubble Breakup in Turbulent Dispersions, *AIChE J.,* **42**:1225-1233 (1996).

[32] Mohammad Pour-Dounighi N., Zolfagharian H., Humoral Immune Response to Diphtheria and Tetanus Toxoids by Intranasal Administration, *Arch. Razi. Inst.,* **61**:81-89 (2006).

[33] Esmaeilnejad Ahranjani P., Kazemeini M., Arpanaei A., Green Biodiesel Production from Various Plant Oils Using Nanobiocatalysts Under Different Conditions, *Bioenerg. Res.* **13**:552-562 (2020).

[34] Zarei M., Shahpiri A., Esmaeilnejad-Ahranjani P., Arpanaei A., Metallothionein-Immobilized Silica-Coated Magnetic Particles as a Novel Nanobiohybrid Adsorbent for Highly Efficient Removal of Cadmium from Aqueous Solutions, *RSC Adv.,* **6**: 46785-46793 (2016).

[35] Sarkar J., Shekhawat L.K., Loomba V., Rathore A.S., CFD of Mixing of Multi-Phase Flow in a Bioreactor using Population Balance Model, *Biotechnol. Prog.,* **32**:613-628 (2016).

[36] Shokri A., Degradation of Terphetalic Acid from Petrochemical Wastewater by Ozonation and O$_3$/ZnO Processes in Semi Batch Reactor, *Arch. Hyg. Sci.,* **6**: 348-355 (2016).

[37] Brumano L.P., Antunes F.A.F., Souto S.G., dos Santos J.C., Venus J., Schneider R., da Silva S.S., Biosurfactant Production by Aureobasidium Pullulans in Stirred Tank Bioreactor: New Approach to Understand the Influence of Important Variables in the Process, *Bioresour. Technol.,* **243**:264-272 (2017).

[38] Kalal Z., Jahoda M., Fořt I., Modelling of the Bubble Size Distribution in an Aerated Stirred Tank: Theoretical and Numerical Comparison of Different Breakup Models, *Chem. Process Eng.,* **35**:331-348 (2014).